Kinematic production of isolated millikelvin molecules

Kevin E. Strecker* and David W. Chandler
Sandia National Laboratories, Livermore, California 94551, USA

(Received 20 March 2008; revised manuscript received 8 August 2008; published 3 December 2008)

Recently we developed a technique for producing cold molecules from a supersonic molecular beam via single collisions with a supersonic atomic beam [M. S. Elioff, J. J. Valentini, and D. W. Chandler, Science **302**, 1940 (2003)]. This cooling technique necessarily produces the cold molecules at the relatively high density crossing of the atomic and molecular beams. In previous reports, secondary glancing collisions with the remnant atomic and molecular beams lead to rapid depletion of the cold molecules limiting the observation time to less than 10 μs with an estimated temperature of 440 mK. Here we present experimental conditions for the kinematic cooling technique which overcome the limitations of the previous experiments. We demonstrate the success of this experiment for the production of cold nitric oxide (NO) in the ground vibrational, $j=7.5$ rotational, state in order to compare with our previously reported data. With the present setup, we are able to extract the cold molecules from the pulsed molecular and atomic beams and we observe these cold $\mathrm{NO}(X)_{j=7.5}$ persisting for over 150 μs. This long observation time demonstrates our ability to temporally and spatially separate the cold molecules from the parent atomic and molecular beams, simultaneously allowing for a better measurement of the final average velocity for the kinematically cooled molecules. From the data we find a final average velocity of the $\mathrm{NO}(X)_{j=7.5}$ of approximately 4.5 m/s, consistent with simulations. The final observed average velocity is equated to a temperature of approximately 35 mK, over an order of magnitude colder than our previous measurements.

DOI: 10.1103/PhysRevA.78.063406 PACS number(s): 37.10.Mn, 37.20.+j, 34.50.Ez

Samples of cold molecules provide a unique environment for controlling and manipulating molecules in isolated quantum states. Like cold atoms, cold molecules, can be manipulated, confined, and stored allowing for the study of exotic states of matter, and detailed information about intermolecular potentials. To date the most successful method for producing cold molecules is "welding" together precooled alkali metal atoms either via photoassociation [1–3] or through manipulation of Feshbach resonances [4–6]. These techniques have been used to realize Bose-Einstein condensation in weakly bound, vibrationally excited dimers [7,8], the observation of Efimov states [9,10], and the exploration of the interface between Cooper pairing and superconductivity known as the BEC-BCS crossover [11–14]. Further, recent photoassociation experiments have produced bi-alkali rovibrational ground-state molecules [15–17].

Cold molecules also offer promise for high-resolution spectroscopy, controlled chemical dynamics, and the study of the long-range interactions between molecules. However, most molecules of interest in combustion, energy, and environmental sciences cannot be synthesized via precooled alkali metal atoms. To address this short fall, several groups have developed techniques to directly slow [18–20], or buffer gas cool [21] molecules. While some of these techniques have proven successful in producing molecules cold enough to trap [21,22], they rely on either favorable electric or magnetic dipole moments of the molecules, or a favorable elastic cross section with a cold He buffer gas.

Here we present results for the molecular cooling technique, "kinematic cooling." In principle, this is a general cooling technique since it relies only on a single collision between the molecule of interest and an atom to bring the molecule to rest in the laboratory frame. The collision occurs in a volume defined by an atomic and a molecular beam intersecting at 90°. The mass ratio of the molecule to the atom along with the initial velocity of the molecule determine the quantum state of the molecule that is cooled. If the masses of the two particles are nearly equal, the cold molecules are produced by elastic scattering and would therefore be in their absolute rovibrational ground state as that is generally what is populated in the molecular beam.

The major obstacle in kinematic cooling is that the cold molecules are necessarily formed in the interaction volume of the two beams. As a result, the cold molecules have a high probability of having secondary glancing collisions with the atomic and molecular beams which can reheat them. Additionally, as the atomic and molecular beams are being turned off they become effusive. Unlike the supersonic beams the effusive beams do not create any cold molecules by kinematic cooling as their velocity is not appropriate, but the effusive beams can reheat the cold molecules. In the past these effusive "afterbeams" have been responsible for the inability to retain cold molecules after the supersonic molecular beams that have produced the cold molecules have been closed. These collisional loss mechanisms limited the observation time of the cold molecules to less than 10 μs.

We report here on our success at reducing the destructive reheating collisions for the cold molecules such that our observation time is consistent with being limited by diffusion of the cold molecules from our interaction region and not secondary collisions. Under the conditions reported here, we are able to observe unconfined kinematically cooled ground vibrational nitric oxide (NO), in the $j=7.5$ rotational state for over 150 μs. An upper limit for the final average velocity is estimated from the diffusion time of the cold molecules from the observation region defined by the intersection of the

*kstreck@sandia.gov

 ©2008 The American Physical Society

atomic and molecular beams with the detection laser. The diffusion of the cold molecules is modeled using a three-dimensional (3D) Monte Carlo simulation to account for the size of the interaction region and laser beam overlap. These simulations are consistent with the data and give an average final velocity of approximately, 4.5 m/s for the $NO(X)_{j=7.5}$. There is no reason to believe that the kinematically cooled molecules are in thermal equilibrium, however, as a matter of convention we use the relationship $\frac{1}{2}mv^2=kT$ to relate the velocity to a temperature. Here v is the average velocity, m is the mass, k is the Boltzmann constant, and T is the temperature. For NO, with a 4.5 m/s final average velocity, one calculates a temperature of approximately 35 mK. This represents a reduction in the observed "temperature" of over an order of magnitude from our previous paper [23]. We are now able to observe a single sample of cold molecules in a field-free region for up to 150 μs which allows for the possibility of high resolution, ~10 kHz, molecular spectroscopy and opens the possibility for trapping of the cold molecules.

Typical cross-atomic-and-molecular-beam (CAMB) experiments operate at the highest atomic and molecular beam densities achievable in order to maximize the signals from weak scattering cross sections. However, in kinematic cooling, we are primarily interested in maintaining the slow molecules for the longest observation times. To understand the effects of the atomic and molecular beam densities on the cold molecules we must determine the production rate of the cold $NO_{j=7.5,\mathrm{cold}}$ while both the atomic and molecular beams are supersonic. This is given by

$$\frac{d(\mathrm{NO}_{7.5,\mathrm{cold}})}{dt} = R_{\mathrm{pro}}(\mathrm{NO}_{j=0.5,\mathrm{beam}})(\mathrm{Ar}) - R_{\mathrm{loss}}(\mathrm{NO}_{7.5,\mathrm{cold}}) \times[(\mathrm{NO}_{j=0.5,\mathrm{beam}}) + 2(\mathrm{Ar})], \quad (1)$$

where R_{pro} and R_{loss} are the respective production and loss rate constants for the cold NO. As the concentration of $NO_{0.5,\mathrm{beam}}$ is only 1% of the Ar concentration, the steady-state condition simplifies to

$$(\mathrm{NO}_{7.5,\mathrm{cold}}) = \frac{2R_{\mathrm{pro}}}{R_{\mathrm{loss}}}[(\mathrm{NO}_{0.5,\mathrm{beam}})]. \quad (2)$$

Equation (2) shows that the steady-state concentration of $NO_{7.5,\mathrm{cold}}$, while the supersonic beams are on, is independent of the Ar beam concentration (as both production and destruction rates of the cold NO are linearly dependent on the Ar beam concentration) and is directly proportional to the concentration of $NO_{0.5,\mathrm{beam}}$. It follows from Eqs. (1) and (2), that the destruction and production rates of the cold $NO_{7.5}$ depend on the Ar concentration while the steady-state concentration does not. Therefore, we can lower the concentration of the Ar to reduce the loss mechanisms associated with the effusive "afterbeams," effecting the time the system takes to reach steady state but not directly effecting the steady-state concentration of the cold molecules. This realization is the basis for the improvements in the experimental conditions reported here.

By varying the stagnation pressure, pulse shape, and pulse length of the atomic and molecular gas valves, we have experimentally determined that the destruction of the cold molecules is most sensitive to the shut off of the atomic and molecular beams as well as the pump out rate of the source chamber between pulses. We attribute this sensitivity to the relatively high density effusive beams which occur during the turn off of the atomic and molecular beams. If the atomic and molecular beams could be instantaneously turned off with no following effusive beams then the steady-state concentration of cold molecules that is present when the supersonic beams are at their peak would be left in the wake of the beams as they flew away. While this ideal situation is not currently attainable, by reducing the atomic and molecular beam intensities we are able to lessen the destructive effects of the effusive beams. The reduced beam intensities mean a lower collision rate at the intersection of the beams, therefore, the beams must be on longer to reach steady state. The cold molecules will build up in the interaction region until the steady-state condition is met. Experimentally, the reduction of the beam intensities is achieved with smaller nozzles for the pulsed valves [24], increasing the distance between the pulsed valves and the interaction region, and reducing the stagnation pressure behind each pulsed valve. A careful balance of all these techniques was explored in order to find the optimal balance between production and destruction of the cold molecules in order to maximize the concentration and lifetime of the observed NO after the atomic and molecular beams have collided.

The CAMB apparatus consists of doubly skimmed crossed atomic beam of Ar and molecular beams of nitric oxide (NO) seeded in Ar. At the core of the CAMB machine is a pulsed atomic beam that intersects a pulsed molecular beam at 90°. The basic construction and operation has been described in detail elsewhere [25]. The atomic and molecular beam valves are each approximately 180 mm from the interaction region. Each valve has a homemade piezoelectric actuator that can open for 150 μs or longer. The gases expand through a 200 μm orifice and each are doubly skimmed by a 700 μm and 1 mm skimmer on their way to the interaction region. A stagnation pressure near 500 Torr was used to minimize the gas load on the chamber while still producing a supersonic flow. The production of cold molecules is monitored by quantum-state selectively ionizing the neutral molecules via $(1+1')$ resonance enhanced multiphoton ionization (REMPI). The NO is excited with one resonant photon near 226 nm on the $NO(A) \leftarrow NO(X)$ transition and ionized with a second photon at 266 nm. The ions are then imaged onto a chevroned microchannel plate coupled to a phosphore screen. The imaging system is operated in "velocity-mapped ion-imaging" mode [26,27] yielding a snapshot of the momentum distribution. The cold molecules are necessarily formed at the crossing of the atomic and molecular beams, and show up near zero velocity on the ion image.

A typical ion image of $NO(X)_{j=7.5}$, with the velocity axis labeled, is shown in Fig. 1. The criteria for the velocity of the NO molecular beam for producing post-collision slow laboratory frame molecules is discussed in detail elsewhere [28]. Here we will only briefly revisit two of the most important criteria. First is the resonance criteria for the internal post-collision energy of a molecule that comes to rest in the laboratory frame,

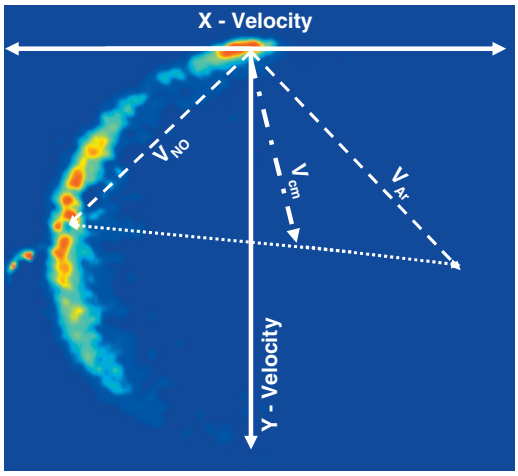

FIG. 1. (Color) Typical ion image of the $NO(X)_{j=7.5}$ with the velocity axis superimposed. $V_{c.m.}$ is the center-of-mass velocity, V_{NO} and V_{Ar} are the laboratory velocities for the NO and Ar, respectively. The bright spot near the origin is due to the coldest molecules. The displayed region is a square region of interest 225×225 pixels or 945 m/s in each dimension.

$$E'_{1_{\text{internal}}} = E_{1_{\text{trans}}}\left(1 - \frac{m_1}{m_2}\right), \tag{3}$$

where $E_{1_{\text{trans}}}$ is the laboratory translational energy of the particle we are attempting to stop, $E'_{1_{\text{internal}}}$ is the post-collision internal energy of a stationary molecule, and m_1 and m_2 are the respective masses of particle 1 and particle 2. Equation (3) dictates that in order to stop a particle in its ground state ($E'_{1_{\text{internal}}}=0$) with elastic scattering, $m_1=m_2$. For colliding systems where $m_1<m_2$, the excess post-collision energy must go into a nontranslational degree of freedom in order for the post-collision particle to come to rest in the laboratory frame. When $m_1>m_2$, the particle with mass m_1 will not be stopped. The second criteria is the post-collision velocity distribution of the slowed particles given by

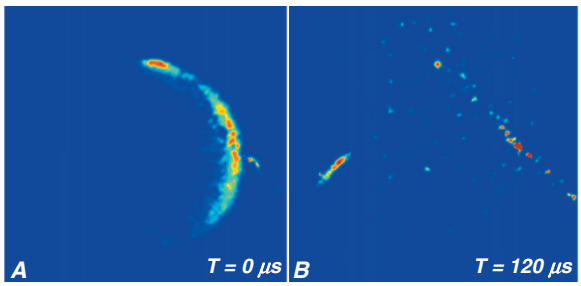

FIG. 2. (Color) Image on the left-hand side is a velocity-mapped ion image of the $NO(X)_{j=7.5}$ at the peak of the scattering between the NO and Ar. All velocity produced during the collision process are visible. The image on the right-hand side is taken after a 120 μs delay. We observe that all the molecules with velocities other than the near zero have flow out of our observation region. Trace amounts of NO are also visible, which originate from the effusion of gas from the source regions.

$$\Delta v'_1/\Delta v_1 = \frac{v_1}{v_{\text{c.m.}}}\frac{m_2^2 - m_1^2}{(m_2+m_1)^2}. \tag{4}$$

Equation (4) gives velocity compression for molecules scattered against the center-of-mass motion. In the case that $m_1 \to m_2$ the post-collision velocity spread tends to zero, but even in the case of $m_1 \neq m_2$, Eq. (4) shows that this scattering technique results in compression of the post-collision velocity spread resulting in an enhanced phase-space density for the cold particles.

In the experiments presented here we use 1% NO seeded in Ar in contrast to our earlier work (5% NO in Ar) in order to slow the velocity of the NO molecular beam such that the cold NO distribution is better centered around zero velocity in the laboratory in concert with Eq. (3). From the velocity-mapped ion imaging we measure an initial translational energy of the NO to be approximately 428 ± 21 cm^{-1}. In order to stop the NO (mass 30) with a collision with Ar (mass 40), Eq. (3) tells us that 25% of the energy must be put into a nontranslational degree of freedom. Therefore, the collision

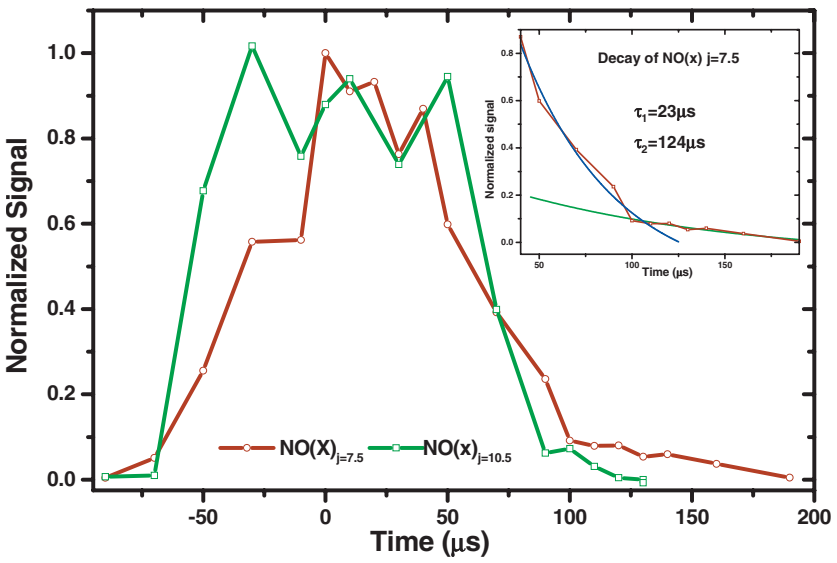

FIG. 3. (Color) Normalized production and decay of the $NO(X)_{j=7.5}$ compared with the $NO(X)_{j=10.5}$. The $NO(X)_{j=10.5}$ data is marked with the □ while the $NO(X)_{j=7.5}$ is marked with the ○. We attribute the loss between 50 and 70 μs to secondary collisions with the parent atomic and molecular beams. The decay from 75 μs and longer is attributed to the cold molecules flying out of the probing region. In this long time region, after 75 μs, we observe a 19 ± 8 μs decay for the $NO(X)_{j=10.5}$ while we observe a longer, 124 ± 4 μs, decay for the $NO(X)_{j=7.5}$. The errors in the decays are found by minimizing the χ^2 value of the exponential fits.

of the seeded NO with Ar must transfer $\sim 106\ \mathrm{cm}^{-1}$ into internal energy. The rotational constant for NO is $1.67\ \mathrm{cm}^{-1}$. The $j=7.5$ rotational state of NO(X) has $106.59\ \mathrm{cm}^{-1}$ of rotational energy. As a result, the fraction of the $\mathrm{NO}(X)_{j=0.5}$ that scatters into the $\mathrm{NO}(X)_{j=7.5}$ against the center-of-mass motion transfers nearly all the residual translational energy into rotational energy and comes to rest in the laboratory frame. The velocity spread of the molecular beam, of 1% NO in Ar, is measured to be approximately 25 m/s. The forces during the cooling process are velocity dependent, and according to Eq. (4) should compress the velocity spread of the cooled $\mathrm{NO}(X)_{j=7.5}$ to approximately 5 m/s.

The velocity-mapped lon imaging is calibrated by photodissociation of O_2 and ionization of the O fragments near 224 nm. This calibration gives resolution of 4.2 ± 0.2 m/s per pixel for NO. The measured resolution combined with 7.8 m/s electron recoil, from the 266 nm NO ionization photon, gives a typical $1/e$ spot size for the cold molecules of 3.2 pixels. This width corresponds to a minimum resolvable temperature of 350 mK for NO, which inhibits direct quantitative velocity measurements for the cold molecules using the velocity-mapped ion-imaging technique. In order to quantify the cooling we obtained in these experiments we define a time $t=0$, such that at time $t=0$, the scattering signal is maximized. The production and fly out of the NO can be monitored as a function of time by delaying the ionization laser with respect to the atomic and molecular beam valves firing. We take a series of images, two of these images are shown in Fig. 2, delaying the ionization laser by a variable amount of time and observing the evolution of the $\mathrm{NO}(X)_{j=7.5}$ molecules. In Fig. 2(b), we observe a spot near the laboratory origin after 120 μs, corresponding to the slowest molecules, the faster molecules have flown out of the ionization volume and are no longer observed.

Figure 3 shows the production and fly out for the $\mathrm{NO}(X)_{j=7.5}$ and the $\mathrm{NO}(X)_{j=10.5}$ quantum states. The data in Fig. 3 is collected by imaging the entire velocity distribution with over 5×10^4 averages, taken with a repetition rate of 15 Hz. The cold molecule signal is selected by taking a square region of interest around the cold molecules ± 10 m/s around the origin. To minimize systematic drifts in the detection laser frequency and power, the data was taken in a nonsequential order, and each point was taken between 2 and 5 times times and averaged together. The detection laser used is a Lambda Physik Scan-mate with a fundamental bandwidth near $0.2\ \mathrm{cm}^{-1}$, pumped by a Coherent Infinity ND:YAG laser with a 5 ns pulse width. The large bandwidth minimizes effects from small drifts in the laser frequency. The cold molecules are produced via collisions between the $\mathrm{NO}(X)_{j=0.5}$ and Ar which have nearly identical pulse shapes. We label the peak of the molecular beam intensity as time $t=0$. The production rate of the cold molecules is proportional to the product of the $\mathrm{NO}(X)_{j=0.5}$ and Ar densities. Measurements of the temporal profiles of the $\mathrm{NO}(X)_{j=0.5}$ and Ar and the number of forward-scattered molecules shows that by $t=70$ μs the production of scattered molecules is below our detection limit while the cold molecules, that are side scattered in the center-of-mass frame, persist. We observe a 124 ± 4 μs decay for the $\mathrm{NO}(X)_{j=7.5}$ at delay times longer than 75 μs.

In Fig. 3 we observe two independent loss rates for each rotational state. The initial rapid loss is independent of the final rotational state and fits to a time constant $\tau = 23 \pm 3$ μs. We attribute this loss to secondary collisions with the atomic and molecular beams as the valves are turning off. The second, longer decay, is rotational state dependent therefore attributed to fly out of the cooled molecules from the interaction region. Exponential fits to the secondary decays give 124 ± 4 μs for the $\mathrm{NO}(X)_{j=7.5}$ (see Fig. 3) and 19 ± 8 μs for the $\mathrm{NO}(X)_{j=10.5}$.

The secondary decays of the cold molecules is modeled using a three-dimensional Monte Carlo simulation to account for the overlap between the detection lasers and the interaction region in which the cold molecules are produced. The interaction region is defined by the overlap of the two doubly skimmed atomic and molecular beams. The lasers bisect the 90° angle between the atomic and molecular beams. By translating the lens that focuses the laser through the beams we can measure the length scale of merit, the long dimension of interaction volume. It is measured to be 540 $\mu\mathrm{m} \pm 20$ μm. The model assumes a square interaction volume in which the cold molecules are produced with a specified average speed and random directions. The detection 226 nm $\mathrm{NO}(A) \leftarrow \mathrm{NO}(X)$ laser, has a measured $\frac{1}{e^2}$ waist of 50 ± 5 μm and a Raleigh range of 3.5 cm. The open diameter of the ion extraction hole in the detection ion optics is 2 cm, and is therefore used as the limiting fly-out dimension along the laser beam axis. In the simulation, the produced cold molecules diffuse, the observed number is recorded at each time step. If a molecule is found inside the laser beam volume, it is detected.

The results of the simulations are compared to the observed secondary decays, shown in Fig. 3. By minimizing the error between the simulation and the observed data, the model gives a final average velocity for the cold $\mathrm{NO}(X)_{j=7.5}$ of approximately 4.5 ± 2 m/s and 58 ± 6 for the $\mathrm{NO}(X)_{j=10.5}$. A second measure of the $\mathrm{NO}(X)_{j=10.5}$ final velocity can be obtained from the velocity-mapped ion imaging. Assuming the $\mathrm{NO}(X)_{j=7.5}$ stationary in the laboratory the spot for the $\mathrm{NO}(X)_{j=10.5}$ appears shifted 14 pixels with a 7 pixel spread. This corresponds to a final velocity of 58.8 ± 14 m/s for the $\mathrm{NO}(X)_{j=10.5}$. We find good agreement between the Monte Carlo simulation, that assumes only diffusion of the kinematically cooled NO(X), and the data. The agreement of the model with the data, along with the vastly different bimodal decay behaviors of the two rotational levels, indicates that the observation time of the cold molecules is limited by fly out rather than secondary collisions with the parent atomic and molecular beams.

Absolute density measurements are extremely difficult under these experimental conditions. However, we estimate the density following Ref. [23], by comparing the background ion count rate to a calibrated SRS RGA-200 residual gas analyzer and correcting for the ionization volume. The ion count rate at the peak of the scattering is about a factor of 5 below our previous results [23] of 10^8 molecules cm^{-3}. Further, we observe that nearly 90% are lost during the molecular beam shut off. We therefore conservatively estimate our final density to be 10^6 molecules cm^{-3}.

For the current experimental conditions the kinematic

equations give a minimum attainable final velocity spread for the $NO(X)_{j=0.5}$ colliding with Ar to produce stationary $NO(X)_{j=7.5}$ of about 5 m/s. For truly stationary molecules in the laboratory frame the 5 m/s velocity spread would correspond to ± 2.5 m/s about the origin. The observed final velocity of 4.5 ± 2 m/s is consistent with the kinematic model, and shows a large improvement over our initial measurements [23]. The final velocity and number of cold molecules depends on the initial beam conditions which were not actively controlled in the current experiment. The final number of molecules is still limited by the residual gas pulse as the pulsed valves are turned off. By constructing valves with sharper turn off times and actively shuttering the beams we hope to further circumvent this loss. Also, temperature controling the pulsed valves will allow for fine-tuning of the initial energy of the NO, thereby tuning the post-collision velocity to ensure the cooled molecules are centered around zero velocity in the laboratory frame.

The primary results of these experiments is graphically summarized in Fig. 3. We have been able to establish a set of experimental conditions such that the cold molecules produced via kinematic cooling are temporally separated from the parent atomic and molecular beams. This conclusion is supported by our observations of the quantum state dependence of the bimodal decays for both the $NO(X)$ $j=7.5$ and $j=10.5$ rotational states. Furthermore, using a 3D Monte Carlo model to simulate the measurements of the slow decays from Fig. 3 we estimate the final average velocity of the cold molecules to be 4.2 ± 2 m/s. Using the velocity temperature relation, we extract a "temperature" of 35 mK for the cold molecules, over a factor of 10 better than our previous measurements which solely utilized the velocity-mapped ion imaging technique. The temporally separated cold molecules can now serve as a starting point for several new experiments including trapping and storing molecules, cold collisional studies, high-resolution molecular spectroscopy, and rotational energy transfer. We are currently working on expanding this technique to other molecular system where molecules can be stopped in their rotational ground state.

[1] R. Wynar, R. S. Freeland, D. J. Han, C. Ryu, and D. J. Heinzen, Science **287**, 1016 (2000).

[2] C. Gabbanini, A. Fioretti, A. Lucchesini, S. Gozzini, and M. Mazzoni, Phys. Rev. Lett. **84**, 2814 (2000).

[3] A. J. Kerman, J. M. Sage, S. Sainis, T. Bergeman, and D. DeMille, Phys. Rev. Lett. **92**, 033004 (2004).

[4] E. A. Donley, N. R. Claussen, S. T. Thompson, and C. E. Wieman, Nature (London) **417**, 529 (2002).

[5] C. A. Regal, C. Ticknor, J. L. Bohn, and D. S. Jin, Nature (London) **424**, 47 (2003).

[6] Kevin E. Strecker, Guthrie B. Partridge, and Randall G. Hulet, Phys. Rev. Lett. **91**, 080406 (2003).

[7] M. Greiner, C. A. Regal, and D. S. Jin, Nature (London) **426**, 537 (2003).

[8] M. W. Zwierlein, C. A. Stan, C. H. Schunck, S. M. F. Raupach, S. Gupta, Z. Hadzibabic, and W. Ketterle, Phys. Rev. Lett. **91**, 250401 (2003).

[9] T. Kraemer, M. Mark, P. Waldburger, J. G. Danzl, C. Chin, B. Engeser, A. D. Lange, K. Pilch, A. Jaakkola, H.-C. Nagerl, and R. Grimm, Nature (London) **440**, 315 (2006).

[10] E. Braaten, H. W. Hammer, and M. Kusunoki, Phys. Rev. Lett. **90**, 170402 (2003).

[11] M. Bartenstein, A. Altmeyer, S. Riedl, S. Jochim, C. Chin, J. H. Denschlag, and R. Grimm, Phys. Rev. Lett. **92**, 203201 (2004).

[12] M. Greiner, C. A. Regal, and D. S. Jin, Phys. Rev. Lett. **94**, 070403 (2005).

[13] T. Bourdel, L. Khaykovich, J. Cubizolles, J. Zhang, F. Chevy, M. Teichmann, L. Tarruell, S. J. J. M. F. Kokkelmans, and C. Salomon, Phys. Rev. Lett. **93**, 050401 (2004).

[14] Guthrie B. Partridge, Kevin E. Strecker, Ramsey I. Kamar, Michael W. Jack, and Randall G. Hulet, Phys. Rev. Lett. **95**, 020404 (2005).

[15] J. M. Sage, S. Sainis, T. Bergeman, and D. DeMille, Phys. Rev. Lett. **94**, 203001 (2005).

[16] M. Viteau, A. Chotia, M. Allegrini, N. Bouloufa, O. Dulieu, D. Comparat, and P. Pillet, Science **321**, 232 (2008).

[17] J. G. Danzl, E. Haller, M. Gustavsson, M. J. Mark, R. Hart, N. Bouloufa, O. Dulieu, H. Ritsch, and H. C. Nagerl, Science **321**, 1062 (2008).

[18] H. L. Bethlem, G. Berden, and G. Meijer, Phys. Rev. Lett. **83**, 1558 (1999).

[19] R. Fulton, A. I. Bishop, and P. F. Barker, Phys. Rev. Lett. **93**, 243004 (2004).

[20] S. D. Hogan, D. Sprecher, M. Andrist, N. Vanhaecke, and F. Merkt, Phys. Rev. A **76**, 023412 (2007).

[21] R. deCarvalho, J. M. Doyle, B. Friedrich, T. Guillet, J. Kim, D. Patterson, and J. D. Weinstein, Eur. Phys. J. D **7**, 289 (1999).

[22] H. L. Bethlem, G. Berden, F. M. H. Crompvoets, R. T. Jongma, A. J. A. van Roij, and G. Meijer, Nature (London) **406**, 491 (2000).

[23] M. S. Elioff, J. J. Valentini, and D. W. Chandler, Science **302**, 1940 (2003).

[24] G. Scoles, *Atomic and Molecular Beam Methods* (Oxford University Press, Oxford, 1992) Vols. 1 and 2.

[25] K. Thomas Lorenz, Michael S. Westley, and David W. Chandler, Phys. Chem. Chem. Phys. **2**, 481 (2000).

[26] D. W. Chandler and D. H. Parker, in *Advances in Photochemistry*, edited by D. C. Neckers and D. H. Volman, (Wiley, New York, 1999).

[27] A. T. J. B. Eppink and D. H. Parker, Rev. Sci. Instrum. **68**, 3477 (1997).

[28] M. S. Elioff, J. J. Valentini, and D. W. Chandler, Eur. Phys. J. D **31**, 385 (2004).